

Dynamic fracture of granular material under quasi-static loading

Amir Sagy,^{1,2} Gil Cohen,³ Ze'ev Reches,^{1,4} and Jay Fineberg³

Received 19 July 2005; revised 14 December 2005; accepted 12 January 2006; published 13 April 2006.

[1] The dynamics of rapid fracturing of heterogeneous grainy media are studied in laboratory experiments in which artificial rock slabs are fractured under uniaxial tension. By performing detailed measurements of the instantaneous fracture velocity and the fracture surface topography, we quantitatively relate fracture morphology with the dynamics of the surface formation. We show that fracture dynamics in these materials is strongly influenced by the interaction of the fracture front with material heterogeneities and by the formation of microbranches. The instantaneous fracture velocity is characterized by abrupt fluctuations, whose amplitudes increase with the average velocity and which are correlated with the surface roughness. The surfaces of the fractures display aligned grooves and ridges, which extend large distances in the propagation direction and are localized in the transverse direction. These features, interpreted as lines of aligned microbranches, are observed solely when the fracture velocity is above 0.3 of the Rayleigh wave speed. In addition, small-scale striations corresponding to fracture front waves are identified. The overall similarity between fracture dynamics in these heterogeneous materials and those in ideal amorphous materials suggests that universal processes control the dynamics. The heterogeneity of the grainy medium, however, strongly amplifies the velocity fluctuations and enhances both the deflection and segmentation of fracture fronts.

Citation: Sagy, A., G. Cohen, Z. Reches, and J. Fineberg (2006), Dynamic fracture of granular material under quasi-static loading, *J. Geophys. Res.*, *111*, B04406, doi:10.1029/2005JB003948.

1. Introduction

[2] The Earth's upper crust contains innumerable fractures that have developed under a wide range of mechanical conditions and velocities [Price, 1966; Kulander *et al.*, 1979; Pollar and Aydin, 1988; Olson, 1993]. In most natural cases, it is difficult to evaluate the conditions that trigger and control the evolution and propagation of fractures. Thus, in the field we have limited information on the instantaneous velocities of propagating fractures, the time and space dependence history of the fracture velocity, or the relationship between the fracture dynamics to the physical properties of newborn fracture surfaces.

[3] Experimental work, on the other hand, has demonstrated that typical structures and morphology develop in brittle homogenous solids that are subject to rapid propagating fractures [e.g., Schardin, 1959; Ravi-Chandar and Knauss, 1984a, 1984b, 1984c; Fineberg *et al.*, 1992; Sharon *et al.*, 1995]. Much of this fracture-induced morphology is independent of specific material properties and loading conditions [Sharon and Fineberg, 1996] and can be

used as a tool to identify and analyze the fracture dynamics [Fineberg and Marder, 1999]. The fracture of grainy materials, such as rocks, is likely to introduce additional complications with respect to the fracture of homogenous, amorphous materials. In grainy materials, fractures propagate in a host material in which the microscopic geometrical and mechanical characteristics vary widely.

[4] There are only a few experimental studies of dynamic tensile fracturing in rock. Most of these studies have focused on "dynamic fragmentation" [Grady and Kipp, 1987] of rock bodies that are subjected to high strain rates. This process is characterized by the spontaneous initiation of many fractures and by pervasive fragmentation of the rock bodies [Grady and Kipp, 1987; Miller *et al.*, 1999]. Measurements of fracture velocities in Norite plates [Bieniawski, 1967] subjected to fast impactors have shown that fractures can achieve velocities of 1.8 km/s, about one half of the shear wave speed. This work indicated that the fracture speed is unstable at high velocities, and that fractures at these velocities tend to bifurcate.

[5] To examine the influence of material heterogeneity on the dynamics of rapid fracture, we performed a series of fracture experiments on plates of artificial rock. The relatively simple experimental system (Figure 1) includes a plate that is subjected to uniaxial tension with constant displacement at its edges (fixed grip configuration). We performed accurate measurements of the instantaneous velocities of propagating fractures and compared them to precise measurements of the associated fracture morphology. The relationships between the fracture morphology and the

¹Institute of Earth Sciences, Hebrew University of Jerusalem, Jerusalem, Israel.

²Now at Department of Earth and Space Sciences, University of California, Los Angeles, California, USA.

³Racah Institute of Physics, Hebrew University of Jerusalem, Jerusalem, Israel.

⁴Now at School of Geology and Geophysics, University of Oklahoma, Norman, Oklahoma, USA.

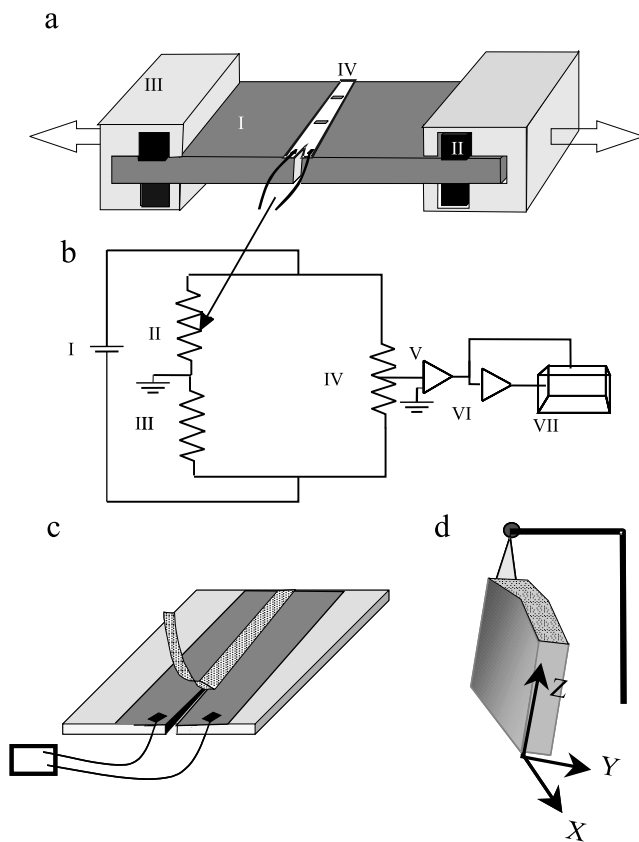


Figure 1. Schematic view of the experimental system. (a) Loading apparatus where the sample (I) is loaded via steel rulers (II) which are glued to the sample. The loading machine grips (III) are operated at constant displacement. Velocities are measured by means of a thin ($\sim 1 \mu\text{m}$ thick) aluminum coating (IV) whose resistance is part of the bridge network shown in Figure 1b. (b) A schematic description of the electrical circuits used: I, Voltage source; II, the resistive layer defined by the aluminum coating in Figure 1a; III, completion resistor; IV, trimmer resistor; V, amplifier; VI, analog differentiator; VII, digitizer. (c) Schematic drawing of the sample calibration method. A conductive tape “rebonds” the two fractured halves of the sample. The tape is then pulled off along the fracture path, while the change in resistance as function of the distance is measured. (d) Scanning laser profilometer and definition of the sample axes.

fracture velocity in the tested grainy materials are then analyzed and compared with that of amorphous materials. Finally, we discuss the implications of our results to fracturing in geological environments.

2. Experimental Procedures

2.1. Experimental Setting

2.1.1. Loading System

[6] All experiments were conducted on plates of artificial rock that were loaded via uniform tensile displacement parallel to the plate in the Z direction (Figure 1), and fractures propagated under constant displacement conditions (Figure 1). During the propagation of the fracture,

the opposing boundaries of the plate in the Z direction were held at a constant displacement such that no additional energy was supplied to the plate. Stress was applied to the sample via massive grips whose ground faces were pressed against steel bars, which were glued to the opposing faces of the sample at each of its vertical boundaries (Figure 1). Both the grips and steel bars were ground to within $10 \mu\text{m}$ tolerances. Tensile stresses, in mode I loading, were applied adiabatically by quasi-static displacement of the grips. The grips are guided by stiff translational bearings mounted on two sets of opposing 50 mm steel shafts to ensure that the loading was only applied in the Z direction.

[7] Prior to loading, a small blunt notch (of length 5–30 mm) located at the midpoint of one of the sample edges, was prepared. The notch served as a controlled fracture initiation point. In our experiments, we increased the displacement of the grips until arriving at a desired value of the applied tensile stress, σ . This initial value of σ is set at a value that is much higher than the minimum value required to fracture the material (Griffith criterion). We are able to ostensibly surpass the Griffith threshold for fracture for the following reason. The Griffith condition assumes that the initial crack is mathematically sharp, yet the initial notch in our samples was quite blunt. As the stress intensity at the notch tip is inversely proportional to the square root of curvature at the crack tip, the finite radius of curvature of the initial notch effectively blunts this singularity. Namely, the bluntness of the notch enables over-stressing of the sample.

[8] The fracture was initiated in one of two scenarios: (1) Spontaneous fracturing, when we waited for the fracture to spontaneously propagate from the notch tip under given applied stress or (2) assisted fracturing, when the fracture onset was externally triggered by forcing two triangular wedges into the initial notch at a selected applied stress. Both of these methods imposed a sharp crack within the already overstressed initial loading configuration. Once this sharp crack was imposed, the system instantaneously found itself beyond the Griffith threshold, and then the fracture would nucleate and accelerate to dynamic velocities, while propagating across the entire sample.

[9] This experimental procedure used is analogous to the loading during formation of joints in the field. First, the field loading rate is quasi-static. Second, natural rocks contain many inclusions and defects, and most of these defects are not geometrically sharp; thus they are not very efficient stress concentrators. Because of this effect, the tectonic loading could exceed the Griffith critical load for sharp defects, and dynamic fractures could develop without dynamic loading.

2.1.2. Velocity Measurement System

[10] Our velocity measurement system (Figures 1a–1c) is a modified version of the system used to measure the propagation speed of mode I fractures in thin plates that was developed by Sharon *et al.* [1995]. They investigated the dynamic instability of a propagating fracture in plates of glass and PMMA. The technique is based on the measurement of the potential drop of a thin ($< 1 \mu\text{m}$) electrically conducting film that is deposited on one or both surfaces of the plate to be fractured (Figures 1a and 1b). As the fracture propagates along the plate, it tears this thin film and thereby changes its electrical resistance. These resistance changes

Table 1. Mechanical Properties of the Different Sample Types Used in Our Experiments

Sample Thickness, mm	P Wave Velocity, m/s	S Wave Velocity, m/s	V_R , Rayleigh Wave Velocity, m/s	Density, kg/m^3	Young's Modulus, GPa	Poisson Ratio
12	4380 ± 82	2520 ± 18	2320 ± 53	2370	37.5 ± 1	0.25 ± 0.01
9	4000 ± 77	2380 ± 25	2120 ± 64	2420	33.6 ± 1	0.22 ± 0.01

Note that the 12 mm and 9 mm thick samples have slightly different compositions.

are solely controlled by the instantaneous position of the fracture tip within the plate, and thus this method provides the instantaneous fracture speed as a function of both the fracture position and time.

[11] The resistance of the thin conductive film is measured by the following procedure. The plate is connected in series with an external resistor, whose value is determined to provide optimal measurement resolution. A constant voltage is applied across this bridge configuration and the instantaneous voltage drop across the sample is measured at a 20 MHz sampling rate and 12-bit resolution during the experiment. From this measurement, we obtain the instantaneous resistance as a function of time during the experiment. As the film's resistance is not linear with the fracture length, resistance-length calibration must be performed for each sample. The resistance-fracture length calibrations were performed by artificially "repairing" the fracture with an electrically conductive tape to bridge the two parts of the broken plate (Figure 1c). The film resistance as a function of the crack length was determined by gradually removing the tape, starting from the fracture initiation point and continuing along the entire fracture path. Combining these results with the real-time measurements provides a high-resolution record of the fracture speed at any time and location along the plate.

2.1.3. Measuring Surface Morphology of the Fractures

[12] The morphology of the fracture surfaces was measured with a scanning laser profilometer made by Optimet LTD. This system measures the fracture surface amplitude (Z in Figure 1d) at each point in X and Y with a resolution of $\pm 1 \mu\text{m}$ (within the fracture plane) and about $5 \mu\text{m}$ in the Z direction. We used the fracture surface amplitudes to calculate RMS surface deviations and geometrical parameters to be described later.

2.2. Experimental Materials

[13] Our experiments were conducted on plates of artificial rock produced commercially from carbonate aggregates cemented by epoxy. The samples are square plates with thickness (Y axis) of either 9 mm or 12 mm, with width (along the Z axis in which the tensile loading is applied), and length (X axis, the direction of fracture propagation) of 400 mm each. The grain sizes of the 9 mm samples ranged from 0.5 mm to 0.05 mm while the grain sizes of the 12 mm samples ranged from 0.2 mm down to 0.01 mm. The artificial rock samples used were quite brittle, and would fracture at applied strains of much less than 0.5%. We chose to use artificial rock plates in our experiments because these plates provide reproducible results due to their homogeneity.

[14] The elastic properties of the samples were determined by direct measurement of the wave velocities of the longitudinal waves V_P , shear waves V_S , and Rayleigh waves V_R . The velocities were measured by 3 MHz ultrasonic transducers and receivers designed for these three types of

waves. The Young's moduli (E) and Poisson ratios (ν) of the samples were calculated from the relations [Landau and Lifshitz, 1986]

$$V_P = \sqrt{\frac{E(1-\nu)}{\rho(1+\nu)(1-2\nu)}} \quad (1)$$

$$V_S = \sqrt{\frac{E}{2\rho(1+\nu)}} \quad (2)$$

The sample density, ρ , was measured by weighing a given volume of sample. Table 1 lists the wave velocities and elastic moduli of the two sample types as denoted by their plate thicknesses. The elastic parameters are similar to typical values of these parameters in brittle carbonate rocks [Farmer, 1983].

2.3. Velocity Data Processing (Postfracture)

[15] Each experiment provided measurements of both the voltage drop (Figure 2a) over the aluminum film during the experiment, $V(t)$, and the temporal derivative, $dV(t)/dt$, of

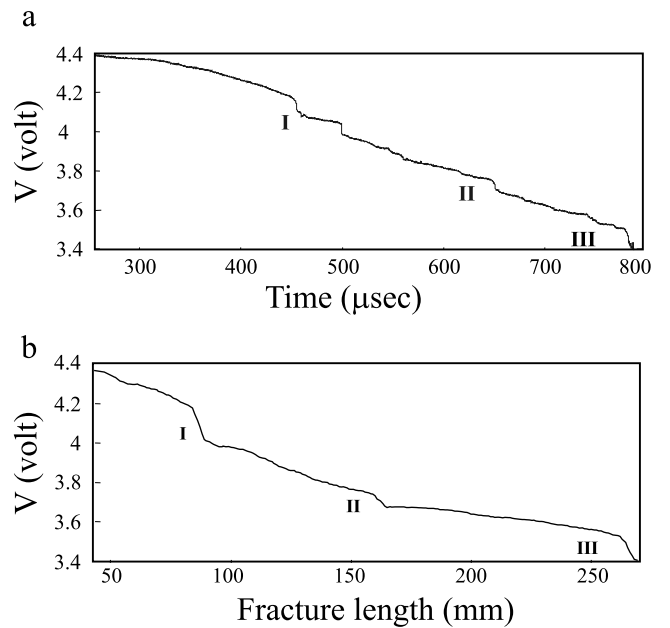


Figure 2. Voltage drop measurements performed in a typical experiment. (a) Time dependence of the voltage drop, $V(t)$, during the fracturing process and (b) the corresponding fracture lengths as a function of $V(t)$ obtained from the postfracture calibration. Voltage drops due to calibration bands (see text) implanted in the conductive layer are labeled (I–III).

the voltage. To calculate the crack velocity, v , as a function of time, $v(t)$, and crack length, $v(L)$, the voltage measurements were first converted into resistance measurements $R(t)$, and, using our calibration measurements (Figure 2b), we obtained the instantaneous crack lengths $L(t)$.

[16] The crack's instantaneous velocity is then given by

$$v(x) = \frac{dL}{dt}(x) = \frac{dL}{dV}(V) \frac{dV}{dt}(V) \quad (3)$$

where dV/dt is directly measured in the experiment and dL/dV is extracted from the calibration measurement, $L(V)$.

[17] We estimate that the measurement accuracies are $\Delta V = \pm 0.001 V$, $\Delta t = \pm 0.1 \mu s$, $\Delta L = \pm 1 \text{ mm}$ (in calibration), and an error of 2–5% in the resistance of the plate. Using these values, the cumulative error in the instantaneous velocity is between 4 and 10% and yields $\pm 5 \text{ mm}$ in the absolute location of the crack tip at any given instant. Our resolution of the relative crack tip locations in a given region is, of course, much better, within 1 mm over a 10–15 cm section. Our measurement accuracy was verified by comparison of the locations of externally introduced localized perturbations to the conductive strip (e.g., local gaps in the conductive film) to the calibrated crack tip locations at these points.

3. Experimental Observations of Dynamic Fractures

[18] We describe here our main observations and their direct interpretation. The velocity variations during fracture propagation are first presented, followed by the fracture morphology and its relations to the propagation velocity.

3.1. Temporal and Spatial Variations of Fracture Propagation Velocity

[19] The voltage drop as function of time and space of a typical experiment are presented in Figure 2. In most experiments, the velocity measurements were performed on a single face of the rock plates used, while in a number of experiments we performed simultaneous velocity measurements on both plate faces. General features of the velocity-length plots (Figure 3) are (1) large velocity fluctuations; (2) initial acceleration of the mean propagation velocity, and (3) until statistically noisy steady state velocities are observed when fracture lengths surpassed scales larger than approximately half of the width of the samples in the Z direction (“strip geometry” [Freund, 1990]).

[20] In most experiments we limited our measurements to the first 200 mm of the sample, to increase our measurement resolution. In experiments in which we extended our measurements to nearly the entire sample width of 400 mm, we found that fractures generally decelerated over the last third of the sample, probably as a result of their interaction with reflected stress waves.

[21] In Figure 3 we present the propagation velocity profile along the fracture path in two typical experiments. In the first experiment (Figure 3a), fracture nucleated at a tensile stress of 4.35 MPa in a 12 mm thick plate with a 24 mm long initial notch. Relatively slow steady state propagation was observed in the first 30 mm with an average velocity of less than $0.2V_R$. The fracture later accelerated to an average velocity of 1.2 km/s, which is

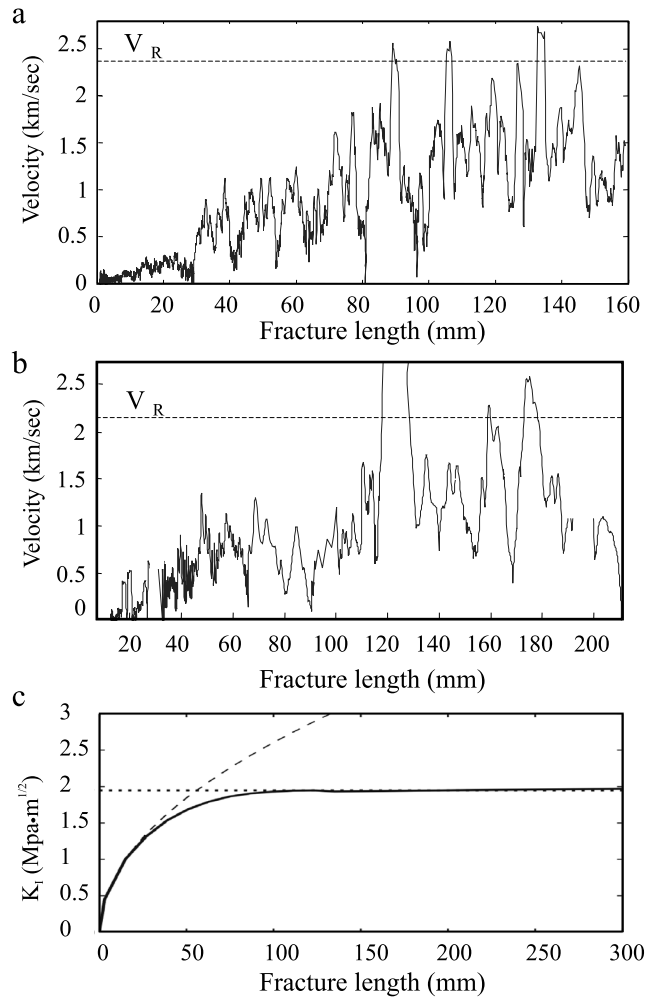


Figure 3. Typical profiles of the instantaneous velocity as a function of the instantaneous fracture length in two different experiments: for (a) a 12 mm width sample and (b) a 9 mm width sample. The final average velocity in both samples is about $0.5V_R$. Note that in both cases a number of velocity fluctuations peaks surpass the V_R limit. Blank sections in Figure 3b surround calibration bands. (c) A plot of the calculated static stress intensity factor, K_I (solid line) as a function of the fracture length, L in a typical experiment. K_I , which is a measure of the loading of the fracture, increases initially according to $K_I = 1.12\sigma(\pi L)^{1/2}$ (dashed line). As the fracture length approaches 100 mm, K_I rapidly approaches the constant value of $\sigma[W/(2-2\nu^2)]^{1/2}$ (dotted line) that is realized in an infinite strip of width W , whose vertical boundaries are displaced by an amount $\sigma W/E$. The K_I presented was calculated for an applied tensile stress of 4MPa for the geometrical dimensions of the samples used in our experiments.

about half of the Rayleigh wave velocity (Table 1). A few typical stages of propagation can be identified in Figure 3. Over the first 10–30 mm, the fracture accelerated continuously with relatively small velocity fluctuations; these fluctuations are on the order of the measurement resolution. As the fracture accelerated to 0.5–1 km/s, the fluctuations increased to magnitudes of hundreds of m/s. Both the mean velocity and the fluctuation amplitudes continued to grow

until the mean fracture velocity reached 1.2 km/s. Although large amplitude fluctuations are observed in this stage, the mean velocity is relatively stable for over 100–150 mm.

[22] It is worth noting that, although the loading was purely quasi-static, the ensuing fractures propagated dynamically, as seen in Figure 3. Rapid (dynamic) fractures were generated in these experiments because, in this loading configuration, the stress intensity factor, K_I that drives the fracture, increases with increasing crack length, L . A typical plot of the stress intensity factor, K_I as a function of L is presented in Figure 3c for this configuration. K_I initially increases rapidly with L , according to

$$K_I \sim 1.12\sigma(\pi L)^{1/2} \quad (4)$$

as in a single edge notch loading configuration [Lawn, 1993] at constant applied stress, σ . This precisely corresponds to the region in Figures 3a and 3b where mean acceleration of the fracture is observed. As L approaches approximately 100 mm, K_I quickly asymptotes to the constant value

$$K_I \sim \sigma[W/(2-2\nu^2)]^{1/2} \quad (5)$$

that is realized in an infinite strip of width W , whose vertical boundaries are displaced by an amount $\sigma W/E$. In this regime, the mean fracture velocity (see Figures 3a and 3b) becomes approximately constant, and the fracture releases an elastic energy of

$$K_I^2/E = G = W\sigma^2/[2E(1-\nu^2)] \quad (6)$$

per unit extension [Fineberg and Marder, 1999].

[23] We now consider the velocity fluctuations of the rapidly moving fractures. In both experiments presented in Figure 3, the instantaneous velocity may either surpass V_R (2.1 km/s), or temporarily fall to nearly zero velocity. In Figure 3b, events of this nature occurred while the mean velocity (between 100 and 200 mm) was 1.13 ± 0.4 km/s ($0.54V_R$). Such large velocities are in contrast with the predicted asymptotic velocity, V_R , of a dynamic crack [Freund, 1990]. Although large fluctuations of fracture speeds have been previously observed in the fracture of nongranular amorphous materials [Sharon et al., 1996], instantaneous velocity values have never been observed to surpass the Rayleigh wave velocity.

[24] To explain these extreme fluctuations, we first examined the voltage drops during the measurements. In all of the experiments in which fracture velocities surpassed V_R , the voltage drops were not smooth, and frequently contained local, nearly discontinuous changes in $V(t)$. These voltage changes were significantly larger than the measurement noise of the system, and also could not be attributed to local changes in the film resistance (as the resistance was about constant at scales of a few millimeters, Figure 2b). Thus the sharp voltage drops reflect genuine changes of the effective fracture speed along the measurement plane. We note that the velocity is measured only at the outer surfaces of the samples, and that velocities averaged over a few centimeters along the propagation direction rarely reach even half of the Rayleigh wave velocity.

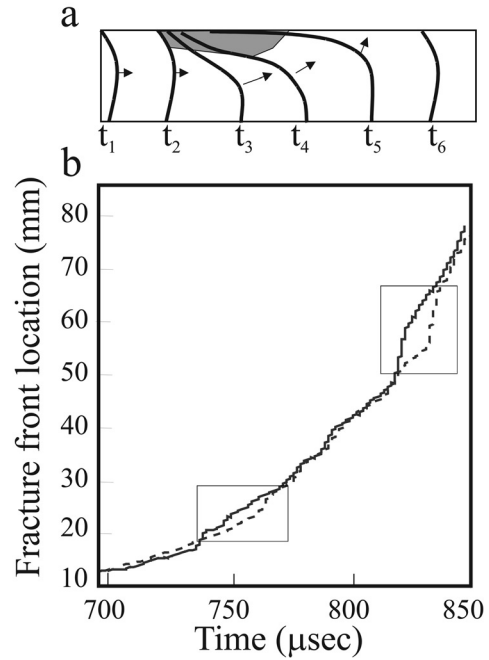


Figure 4. (a) A schematic drawing of our explanation of the anomalously high ($V > V_R$) velocity fluctuations demonstrated in Figure 3. When the fracture front (black lines) crosses a strong inhomogeneity (grey area), the front is diverted, with both its direction and instantaneous velocity locally changed. This will be measured on the upper surface as an extremely large instantaneous fluctuation in the velocity (deceleration and acceleration in this simple case). Although the propagation velocity is less than V_R , the apparent velocity, as measured on the upper surface, may well surpass V_R . (b) Simultaneous measurements of the location of the fracture front on both faces of a sample as a function of time. Each face is marked by a different line style. The rectangles denote “bubbles” in which the front is noticeably crooked and a gap is created in the relative front positions on the two faces of the sample.

[25] These anomalous velocities could occur when the fracture front locally loses its original shape, that of a “straight” fracture front oriented normal to the propagation (X) direction. We will show that, possibly as a result of its interaction with material inhomogeneities, the crack front becomes diagonal or even discontinuous. This picture is demonstrated schematically in Figure 4a. Three different observations provide support for this assumption: (1) in this picture one would expect to observe a phase of slow or even arrested effective propagation either immediately before or after a large voltage drop anomaly (Figure 4a) to compensate for the accelerated phase; (2) if the fracture front “breaks”, the location of velocity anomaly should be different at the two outer faces of the plates; and (3) if these anomalous voltage drops were caused by branching events, they will affect the local roughness of the fracture surface.

[26] We examined the behavior of many samples in light of these predictions. We indeed found that the local anomalous voltage drops (velocity increases) were either preceded or followed by a slow propagation phase. In Figure 4b we show

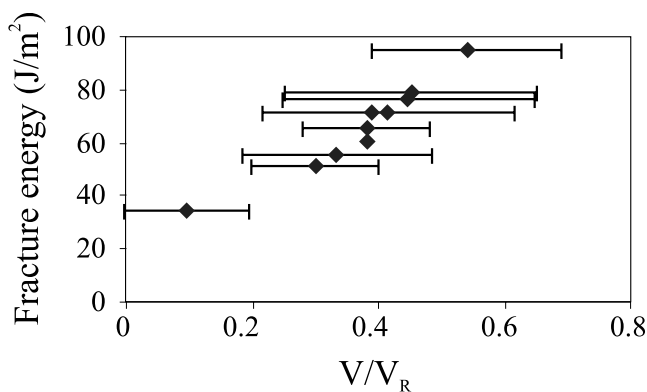


Figure 5. Energy flux (energy release rate) into the fracture tip (G) as a function of the average steady state final velocity. Data were taken from ten experiments in 9 mm width samples (see text).

the simultaneous locations of a fracture front at both faces of the sample, as a function of time for an experiment in which anomalously large values of the fracture velocity were observed. In this experiment, the plate was coated with conductive films on both faces and the voltage drops on each face of the plate were independently measured (Figure 4b). On average, the location of the front during propagation at both sides of the sample is the same, implying that, on average, the fracture front is oriented normal to the propagation direction, as expected. Locally, however, the time-dependent location of the front at each side shifts rapidly and large local gaps in the location of the fronts on either side of the plates develop. In Figure 4b, such gaps are clearly recognized at two locations by a 2–4 mm difference in locations between 20 and 30 mm and by up to a 12 mm difference at locations between 50 and 65 mm. In both of these cases, the front “corrects” its shape and propagation direction after a few millimeters. This observation suggests that the front remained skewed over distances of a few millimeters and corrections to this skew gave rise to the effectively “instantaneous” propagation in the Y direction that leads to the extreme “anomalous” velocities that we measure.

[27] Contrasting the present experiments to those in amorphous materials, we assume that the extreme velocity fluctuations observed here (and not observed in ideal materials) are triggered by either the heterogeneity of the host material and/or by branching events. In the next section we will show that these ideas are confirmed by surface roughness and fracture morphology analysis.

[28] Let us now consider the fracture energy of the material as a function of the propagation velocity. In general, the fracture energy in many materials increases rapidly with the mean propagation velocity [Fineberg and Marder, 1999]. In amorphous PMMA, Sharon *et al.* [1996] demonstrated that this velocity dependence can be entirely understood by the increase of the fracture surface area, when the additional fracture surface due to subsurface branching is taken into account. In Figure 5 we present the measured values of the fracture energy in our experiments as a function of the mean velocity in 10 experiments performed on the 9 mm thick samples. In these measure-

ments we consider only values of the velocity (and consequent fracture surface) formed when the system propagated in a statistical steady state regime, after the initial acceleration phase. This occurs after the fracture has propagated 80–100 mm, and K_I approaches a constant value (see Figure 3c). Once the velocity is, on average, constant, the velocity-dependent kinetic energy radiated by the moving fracture is also constant. The fracture energy can then be calculated, as by Sharon *et al.* [1996], by using the effective translational invariance of the system in this regime. In this steady state regime, the net fracture energy released per unit extension is simply equal to the strain energy per unit length of the uniformly displaced system far ahead of the fracture tip [Freund, 1990], $W\sigma^2/[2E(1-\nu^2)]$, as given by equation (6). This dissipated energy is not necessarily independent of the value of the fracture velocity and, as shown in Figure 5, a strong velocity dependence of the fracture energy is evident. Although we have no direct evidence for this, it is conceivable that this increase in fracture energy with v may also be explained by the formation of subsurface structure precipitated by frustrated branching events, since this increase in fracture energy with v is accompanied by large velocity fluctuations that are known to accompany microbranching in ideal materials.

3.2. Fracture Morphology

[29] In this section, we present observations, measurements and interpretations of the fracture surface topography. The fracture surface data provides indicators for the development of roughness patterns, and it reveals the relations between surface morphology and the dynamics of the propagating fracture.

3.2.1. Fractographic Analysis

[30] Figure 6a displays typical views of the surface morphology at low velocities (0.2–0.3 km/s) on the left and high average velocities (0.8–1.2 km/s) on the center and right. The photographs reveal patterns of holes and ridges with accompanying striations that start to become visible at average velocities beyond $\sim 0.3 V_R$. At higher average velocities, these features are more pronounced and their size roughly increases with the velocity (Figures 6b and 6c). One of the dominant features of the fracture surfaces is the appearance of sets of subparallel and cross-cutting topographic bands. Figure 6d is a color map of the first 200 mm of a fracture surface along which the fracture accelerated from rest to a mean velocity of 0.8 km/s ($0.38 V_R$ in the 9 mm thick sample). The general increase of the surface roughness with fracture velocity (and distance) is evident by the increase of the color range from left to right. Distinct band-like structures that are aligned at acute angles to the mean propagation direction of the fracture are clearly observed in Figures 6d and 6e. These structures are typical of the $v > 0.3 V_R$ sections in all our samples. Close inspection of a single band reveals that it contains chains of holes and ridges which are aligned along the band. We interpret these ridges and holes as directed lines of microbranches, or branch lines that are aligned in the propagation direction.

[31] The development of similar branch lines was documented in dynamic fractures in soda-lime glass [Sharon *et al.*, 2002], and in brittle polyacrylamide gels [Livne *et al.*, 2005]. The latter study showed that many of the branch

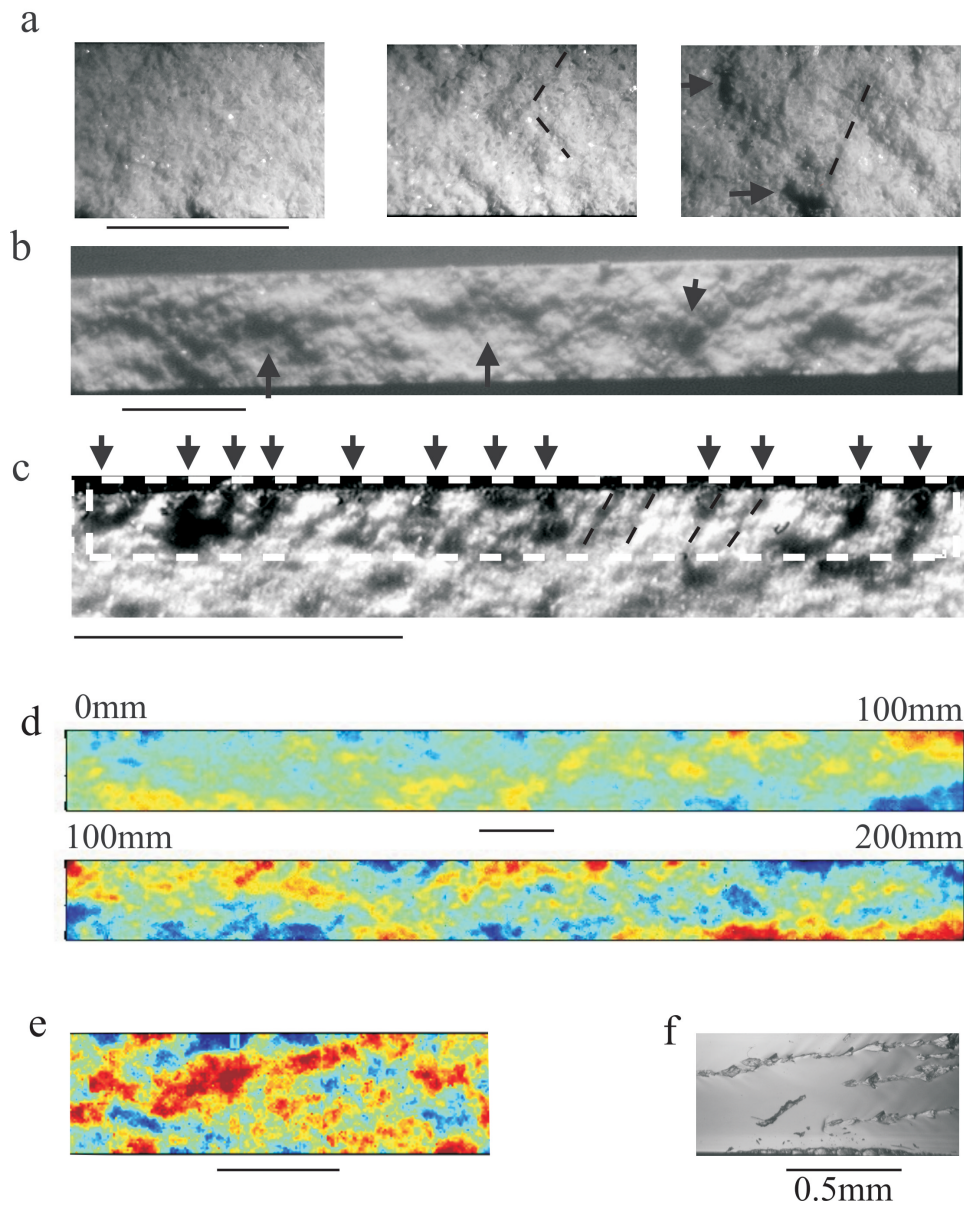


Figure 6. Topographic pictures and maps of typical fracture surfaces. (a) Photographs of the fracture surface of a typical sample (9 mm width) at different locations (velocities). (left) Near the fracture initiation point ($V = 0.05\text{--}0.15V_R$), the surface is smooth down to the scale of the grain size (the “mirror area”). Holes, ridges and striations (center and right) appear when $V > 0.3V_R$. (b) Patterns created by a fracture that propagated at mean velocities in excess of $0.55V_R$. Large holes (microbranches) noted by the arrows are apparent. (c) A branch line near the upper part of the fracture surface (enclosed by a white dashed line) in a 12 mm wide sample. Small-scale striations are also observed. In Figures 6a–6e, horizontal black lines note a 1 mm scale. Dashed lines highlight representative striations; black arrows, ridges/holes. (d) Maps of the first two 100 mm sections of a sample in which the fracture accelerated from standstill to an average final velocity of $0.38V_R$. The intensities represent different heights (deep blue, -6 mm; deep red, 6 mm). Aligned ridges (red colors) and holes (blue colors) appear along the surface from 90 to 200 mm. (e) Diagonal patterns cross the surface formed by a fracture propagating at a mean velocity of $V = 0.45V_R$ (deep blue, -4 mm; deep red, 4 mm) These patterns are similar in their shape to the branch lines observed in the fracture of (f) poly acrylamide gels. The photograph in Figure 6f is courtesy of A. Livne.

lines in brittle gels are often tilted at slight angles from the X direction (Figure 6f) or develop near the sample edges, in a similar way to those observed in our experiments. In these three materials (glass, gel, and artificial rock), the branch

lines only develop when a fracture front propagates at high velocities.

[32] The subsurface features, generally identified as microbranches in optically transparent materials [Sharon

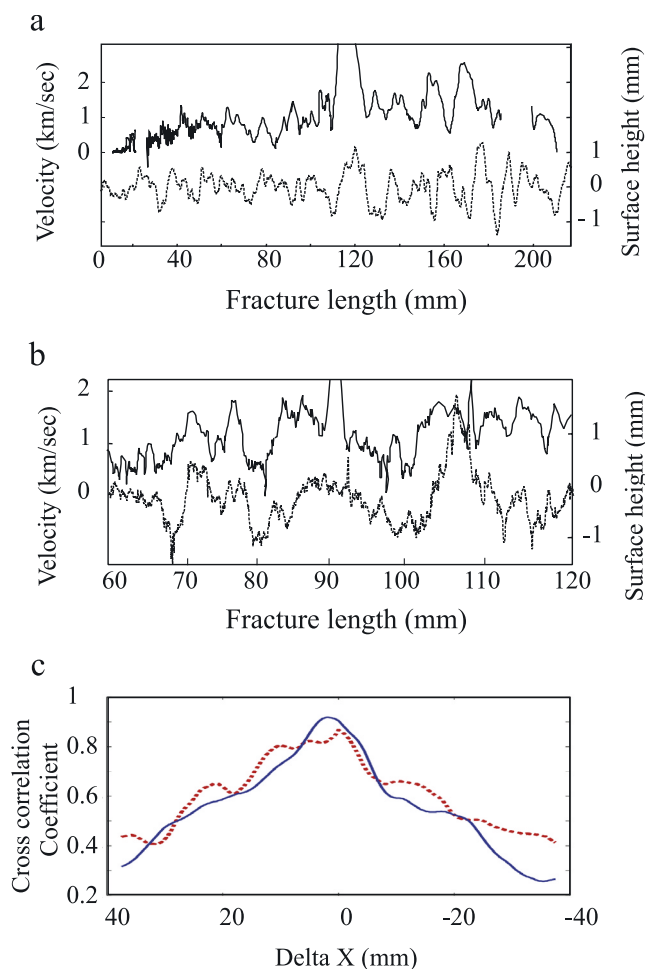


Figure 7. (a, b) Correlation between surface amplitudes (dotted lines) and velocity fluctuations (solid lines) in two different experiments. Shown are the average amplitudes (dotted lines) of 50 adjacent XZ profiles (spanning about 1 mm in the Y direction) near the upper surface, where the velocity (solid line) was measured. (c) The cross correlation between the velocity and surface amplitudes yield maximal correlation coefficients of 0.88 for the sample in Figure 7a (dotted line) and 0.93 for the sample in Figure 7b (solid line). Such clear correlations are only observed when a branch line develops in close proximity to the velocity measurement plane (see Figure 6c). Note that the correlations are clearly evident at widely different scales.

et al., 1996], could not be directly observed in our non-transparent materials. On the other hand, fracture surface features that are characteristic of microbranches, e.g., branch lines [Sharon *et al.*, 2002; Livne *et al.*, 2005], are also readily observed in our samples (Figure 6). These observations and the distinct association between velocity and roughness (see below) allow us to identify the aligned holes and ridges, such as those presented in Figure 6, as microbranches that exist within branch lines.

[33] Figure 6b shows the fracture surface created in the final stages of very rapid fracture. Large microbranches with dimensions of 4–5 mm develop on the surface. The occurrence of such large microbranches is generally correlated with the large fluctuations in fracture velocity, such as

those presented in Figure 3. When large microbranches were observed, it was difficult to accurately determine the instantaneous speed within the corresponding fracture velocity measurements due to the large velocity fluctuations at these locations.

3.2.2. Surface Roughness

[34] We calculated three parameters that characterize the roughness of fracture surfaces, and examined the relations between the fracture velocity and the surface topography. The parameters are (1) the total area of the fracture surfaces; (2) direct measurements of detrended fracture surfaces adjacent to the plate surface where the velocity was measured; and (3) the RMS variation of sections of the fracture surface topology as a function of their location along the fracture surface.

3.2.2.1. Fracture Area

[35] Analysis of a number of samples (9 mm in width) demonstrated that after removing large-scale trends (for $\Delta X > 10$ cm) the total increase in surface area of a single fracture surface is between 5–12%, with respect to a flat surface. Measurement of featureless “mirror” zones indicated a 3–5% increase of surface area, while along branch lines the surface area increases by 10–15%. We found that the total surface area systematically increases with the fracture velocity (e.g., Figures 6a and 6d). Total increases of fracture surface greater than 7% were observed only for fracture velocities greater than $0.5V_R$. Quantitative comparison of the fracture surface area increase with the velocity fluctuations is difficult, since it is impossible to objectively “filter out” the huge velocity fluctuations caused by propagation of the fracture front in the “Y” direction (as noted previously). Qualitatively, however, the relative increase of the fracture surface area seems to be correlated with the increase in both the frequency and amplitude of the velocity fluctuations. Quantitative comparisons, as we will show in the next section, were possible in sections of the fracture surface where branch lines were observed to propagate in the X direction at Y locations adjacent to the sample faces where velocities were measured.

3.2.2.2. Relations Between Propagation Velocity and Surface Topology

[36] Correlations of the surface topography to the fracture dynamics were examined by comparing Z values of the fracture surface topology as a function of X with the corresponding velocity fluctuations at different spatial scales. To reduce the effect of surface features related to the samples’ grainy character, profiles were averaged over thin zones in the Y direction. The width, ΔY , of these zones was on the order of 1 mm (50 adjacent X–Z profile measurements). This scale is an order of magnitude smaller than the overall sample widths, but significantly larger than the samples’ grain sizes.

[37] Plots of surface topography variations together with the corresponding instantaneous fracture velocities are presented in Figures 7a and 7b. The data, from two different experiments, are taken from sections in Y that are adjacent to the velocity measurement planes. Velocity and surface fluctuations can be highly correlated. In the two data sets, correlations over scales ranging from slightly larger than 1 mm to scales of over 20 mm are apparent. As demonstrated in the cross-correlation functions presented in Figure 7c, a large degree of correlation is observed between,

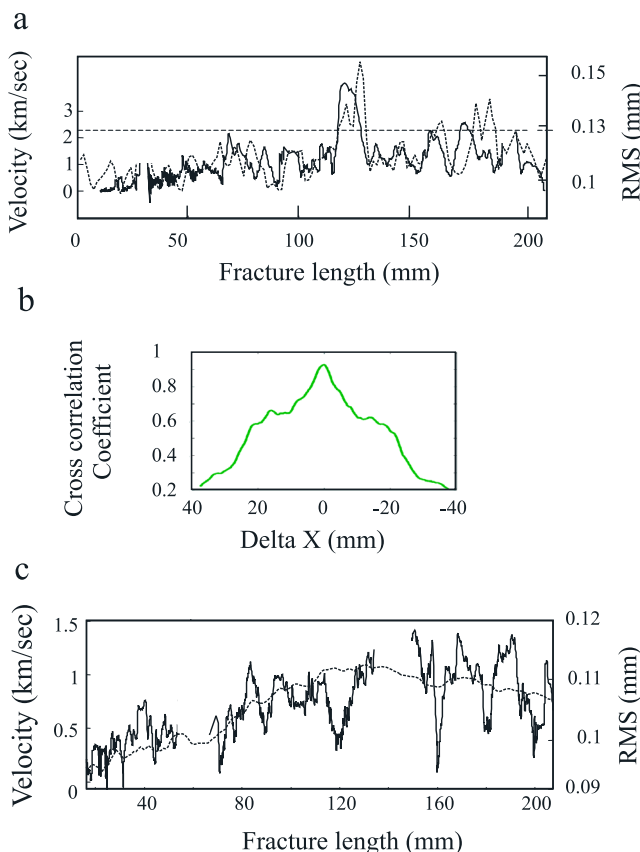


Figure 8. Correlations between the RMS surface fluctuations (dotted lines) and fracture velocity fluctuations (solid lines). Each RMS value is calculated for an XY section of size 10 mm \times 9 mm (see text). (a) and (c) Local values of RMS surface fluctuations and velocity fluctuations in different experiments. (b) Cross-correlation analysis between velocity and surface RMS of the data in Figure 8a. Correlations of the mean RMS values with the velocity, shown in Figure 8c, are more typical. Note that the large fluctuations in the RMS surface measurements in Figure 8a correspond to anomalous velocity fluctuations which exceed V_R (dashed line).

for example, the locations of peak values of the surface height and those of the velocity fluctuations. Such correlations are visible both at relatively large scales (e.g., from 80 to 180 mm in Figure 7a, with large correlated fluctuations at the 10–20 mm scale) and small scales (fluctuations down to 5 mm scale, from 70 to 110 mm in Figure 7b). As spatial averaging of the data is performed over scales of order 1 mm, correlations smaller than this scale are wiped out. It is conceivable that these correlations persist down to the material grain sizes. In most measured samples, the largest amplitude variations of the surface topology are observed at scales of 5–20 mm in the X direction.

[38] It is interesting to note that, in all of these data, there is a strong correlation not only in the amplitudes of the fluctuation but also in the relative phases of the fluctuations (Figure 7). In other words, successive maxima (minima) in the surface amplitudes correspond to successive maxima (or minima) in the velocity fluctuations. These nontrivial phase correlations suggest that the fluctuations are not random, but

that long-range correlated behavior persists over large regions (100–200 mm in Figure 7a) that are on order of the overall sample size (400 mm). These long-range correlations suggest that the same dynamics that leads to the velocity fluctuations gives rise to the fracture surface formation. The phase correlations indicate that the dynamics retains a “memory” of past events over scales which are much larger than either the grain size or sample thickness.

[39] It is important to emphasize that strong correlations between the velocity fluctuations and the surface amplitudes were visually apparent when (1) the measured fracture surface is adjacent to the velocity measurement plane and (2) when branch lines, parallel to the propagation direction, were generated near the velocity measurement plane, as, e.g., in Figure 6c. Sections of the fracture surface which are farther than a few millimeters from the velocity measurement plane exhibit much lower degrees of phase-correlated behavior. Such strong correlations between surface structures along the velocity measurement plane have previously been observed in the fracture of amorphous materials. For example, in glass, velocity fluctuations (in both phase and amplitude) have been observed to correlate with fracture surface heights [Sharon *et al.*, 2002]. Similar correlations between velocity fluctuations and the appearance and lengths of microbranches were noted in PMMA [Sharon *et al.*, 1995]. In the experiments in glass, the velocity fluctuations were attributed to front waves, which were generated by either branching events or external perturbations. In subsequent sections we will present evidence that a similar picture may also explain the generation of surface structure in our experiments.

3.2.2.3. Relations Between Velocity Fluctuations and RMS of Surface Topography

[40] In the previous section we showed that a clear correlation between velocity fluctuations and surface structure exists, but noted that this correlation decays rapidly with the distance in Y from the velocity measurement plane. We saw that these direct correlations were most readily apparent in the relative phase of these fluctuating quantities. Here, we concentrate solely on the amplitude fluctuations of both the velocity and surface structure. Technically, this is performed by comparing the RMS variations of the surface structure with the velocity measurements.

[41] The RMS variations of the surface structure were calculated for different $\Delta X \cdot \Delta Y$ sections along the fracture surface where $\Delta X = 1\text{--}20$ mm and ΔY was the entire sample width. The calculations were performed for overlapping sections in the X direction that spanned the entire fracture surface, with varying degrees of overlap between adjacent sections. The most pronounced correlations appear when the averaging is performed over section sizes of $\Delta X = 5\text{--}15$ mm, which are equivalent to 50–150 grains. The correlations diminish for larger section sizes, probably due to smearing of the velocity and surface fluctuations. At smaller section sizes, the inherent grain heterogeneity dominated the surface fluctuations, and the correlations with velocity fluctuations are obliterated.

[42] The strength of RMS correlations varied significantly from sample to sample, and two typical comparisons are presented in Figure 8. In some cases, excellent local correlations between RMS surface fluctuations and velocity fluctuations could be found over large distances on the

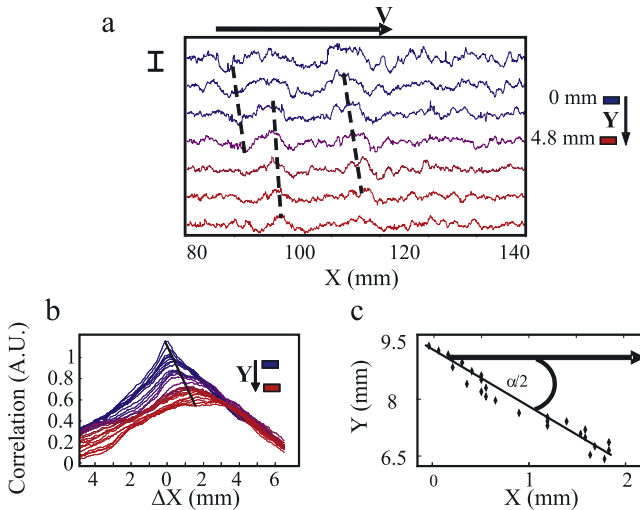


Figure 9. Application of the cross-correlation method to the fracture surface. (a) Plots of successive XZ profiles along an XY section of size 60 mm × 4.8 mm taken from within the 12 mm thick sample presented in Figure 6c. The scale in Z is indicated by the 0.5 mm bar to the left. Successive profiles are spaced at $\Delta Y = 0.8$ mm intervals. Amplitude perturbations (in Z) are seen to propagate in the X direction with increasing Y. A few specific propagating perturbations can be followed (noted by dashed lines). (b) Cross correlation of 30 successive profiles, spaced at intervals of $\Delta Y = 0.1$ mm, along a 3 mm thick section chosen from the area presented in Figure 9a. For increasing Y, the peak correlations are both shifted in the X direction and decreasing in amplitude. (c) A plot of the correlation peaks in Figure 9b demonstrating that the peaks trace out a straight line. When using the relation $V = \cos(\alpha/2)$ (by assuming that the propagation of the perturbations is due to front waves; see text), we find that the average velocity of this section is $0.52V_R$, which is consistent with the directly measured value of the velocity.

surface (Figures 8a and 8b). In these cases even the short-scale (5–10 mm scales) fluctuations of the fracture velocity are echoed in the RMS surface height measurements. The rough correlations evident in Figure 8c are, however, more typical. Here, correlations over larger (30–40 mm) scales were more evident, with those at small scales smoothed out. The differences between different samples are affected by the number and scales of the dominant surface features formed in a given experiment.

[43] In some samples, such as that presented in Figure 8a, the strong local correlations between the short-scale velocity fluctuations and RMS surface measurements (Figure 8b) suggest that most of the surface fluctuations were generated by dominant surface features that extended throughout the width of the sample. One of the more striking features of the fracture presented in Figure 8a is that the large RMS surface anomalies correlate well with anomalies in the velocity fluctuations. These observations, together with the strong correlations between peak-to-peak amplitudes and velocity fluctuations (Figure 7), suggest the following process. Anomalously high velocities develop when the fracture front is “broken” discontinuously. This break-up occurs

due to the formation of either a large-scale branch (Figure 7b) or the interaction of the front with a large inhomogeneity. We assume that when such break-up of the fracture front occurs, the surface roughness amplitude (and the associated RMS) increases, and the direction of the front may be diverted. This process generates a local velocity component in the Y direction (Figure 4a) and associated extreme velocity fluctuations when the diverted front cuts through the velocity measurement plane at the sample’s faces. This scenario suggests that branching events are the major source for the correlation between fluctuation in the velocity and in the fracture roughness, as well as the observed anomalous velocities.

3.2.3. Analysis of Front Waves Traces

[44] The fracture surfaces display additional small-amplitude features that differ in size, shape and orientation from the microbranches. These features are patterns of elongated striations, with lengths of up to a few millimeters and widths of less than 0.1 mm (dashed lines in Figures 6a and 6c). These striations form V-like patterns (Figure 6a) that radiate away from their starting points toward the sample edges. Their dimensions are small compared to the width of the sample. Direct analysis of these features is difficult, as they only slightly protrude above the background roughness determined by the grains.

3.2.3.1. Identification of Front Waves

[45] Sharon *et al.* [2001] demonstrated that front waves (FW) are initiated by microbranches or asperities that generate two counter-propagating pulses moving with velocity V_{FW} relatively to the medium. The FW can be identified as two tracks along the fracture surface that enclose an angle α defined by:

$$\cos(\alpha/2) = v/v_{FW} \quad (7)$$

when the fracture front is normal to the direction of propagation. If the front is oriented at an angle β relative to v, then:

$$v/v_{FW} = \cos(\alpha/2)/\cos(\beta) \quad (8)$$

[46] This type of direct identification is difficult in granular samples, as every large grain can act as a FW source. Thus an ensemble of front waves is generated at any given instant. We use the method below to identify the “mean” propagation of ensembles of FW within small regions of the fracture surface.

[47] We first consider topographic profile lines in the X direction (Figure 9a) that are averaged over a range, ΔY , much smaller than the sample width. We then search for the best correlation between a given (reference) profile, and successive profiles in the Y direction; seven such profiles are plotted in Figure 9a. The reference profile can be chosen anywhere along the surface. The cross correlations between the reference profile and each successive profile in the Y direction are calculated as a function of a shift, ΔX , in the X direction. A traveling or propagating feature will be manifested as a peak of the cross-correlation plot at a nonzero value, ΔX_{peak} , of ΔX . A linear fit of $\Delta X_{\text{peak}}(Y)$ with Y will yield the propagation velocity of the wave ensemble. This analysis further provides the rate of decay of the FW with distance.

[48] This cross-correlation analysis of the fracture surface enables us to answer three central questions:

[49] Are the perturbations that traverse the fracture surface coherent waves?

[50] What is the length (or lifetime) of a perturbation?

[51] Do the shifted perturbations create well-defined angles, and if so, are these angles related to those predicted for front waves?

[52] Figure 9b presents an example of the cross correlations within the section presented in Figure 9a. The reference profile was chosen to be the profile with the largest fluctuations within the examined section. Figure 9 demonstrates the continuity of correlation along 30 profiles extending over $\Delta Y = 2.5$ mm. The cross correlation between the profiles yields a continuously propagating peak that is noticeable for least 2.5 mm. The graph demonstrates that the location in X of the perturbation (i.e., the location of the maximal cross correlation) is shifted in every profile. The maximum correlation amplitude of each profile decays systematically with increasing Y. The points of the maximal correlation amplitude (Figure 9c) trace a straight line, as expected for a FW [Sharon *et al.*, 2001]. We determined the average angle traced by the propagating ensemble of striations by linear regression of these points.

3.2.3.2. Testing the FW Striations

[53] Finally, to test the hypothesis that the shifted perturbations are formed by FW, we measured the existence and orientation of such propagating perturbations along consecutive sections of the fracture surface. Figure 10 displays the results of the cross correlation measurements along a 50 mm length of one fracture surface. At each point in Figure 10, the velocity was calculated using equation (8), where the propagation angle, α , was determined in the above procedure for a rectangular section of 20 mm by 2.8 mm. Each sequential rectangular section was chosen to overlap half of the previous one to both improve the statistics and to increase the number of points along the sample. This calculated velocity is compared with the mean velocity within each corresponding section that was measured by the voltage drop method during the experiment (Figures 10a–10c). This comparison demonstrates that the velocities obtained by means of cross correlation measurements for propagating front waves mirror the measured velocities.

[54] Application of the above procedure to the fracture initiation region ($L < 50$ mm), where the fractures rapidly accelerated, was less effective. In this region, the perturbations are initially smaller and they fade relatively rapidly, with many of the profiles in the noise levels. We found, however, that by averaging measurements performed using different reference lines (Y), at the same location in X, we were able to reliably measure the propagation angles of perturbations within the acceleration stage by the cross-correlation method (Figure 10c). As in the steady state propagation region, these results provide good quantitative agreement between the measured velocities and those obtained by these cross correlations.

[55] In some cases, we identified two directions of perturbation propagations that resemble the V-like patterns formed by counter-propagating FWs observed in amorphous materials [Sharon *et al.*, 2002] and in the analysis of shatter cone formation [Sagy *et al.*, 2002, 2004]. Using equation (5), these observations could be used to measure

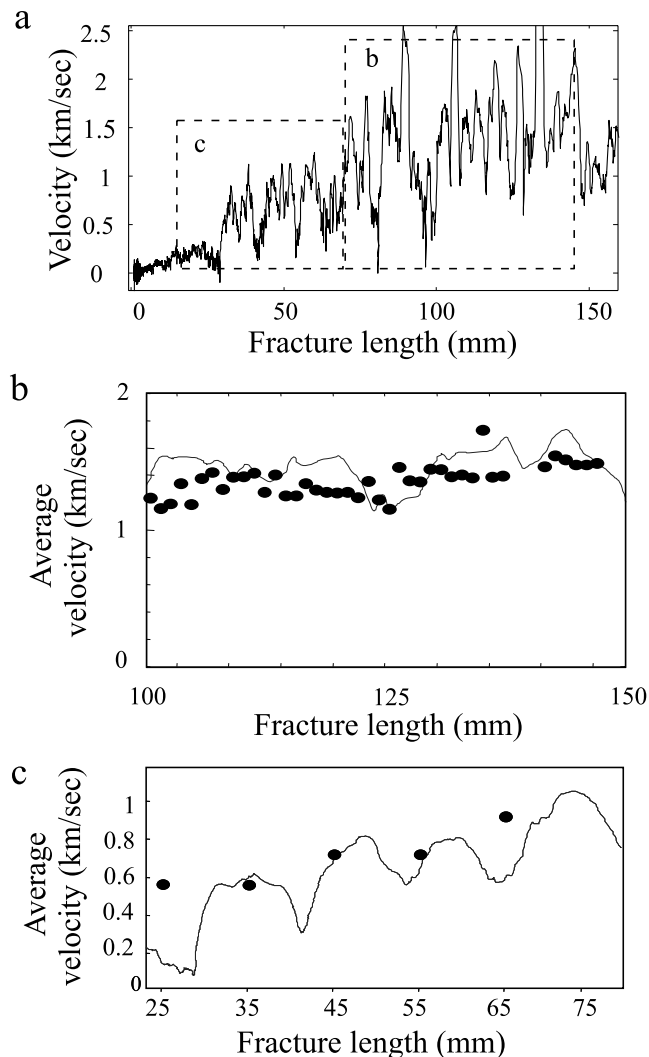


Figure 10. Velocity measurements using the cross-correlation method in two sections along a single fracture surface (using a 12 mm width sample). (a) Velocity measured in the experiment (as in Figure 3). The dashed areas denote the two sections which are analyzed in Figures 10b and 10c. (b) and (c) The plots comparing the velocity, as calculated using the cross-correlation technique (points), to measured mean velocities at the upper surface (line). Each point in Figure 10b is the velocity calculated from a propagation angle obtained from the cross-correlation measurement taken in a rectangular section having dimensions $\Delta X = 20$ mm and $\Delta Y = 2.8$ mm. Each sequential rectangular section overlaps half of the preceding one. In Figure 10b, the reference line (see text) is located in the near proximity of a branch line while in Figure 10c (to improve accuracy) each point is the average (in Y) of measurements using 15 different reference lines.

the angle of the front with respect to the main axes (X, Y) of the sample.

3.2.3.3. Front Waves and RMS Fluctuations

[56] Understanding the effects of random perturbations to a crack front on the front integrity, was one of the motivations for the theoretical derivation of front waves. Both scalar [Perrin and Rice, 1994; Ben-Zion and Morrissey,

1995] and vector models [Morrissey and Rice, 1998, 2000] predicted that the RMS roughness of a crack front should increase in time (at a constant fracture velocity) as a result of the interaction of the front with sample inhomogeneities. The vector (realistic) model of tensile (mode I) fracture by Morrissey and Rice [1998, 2000] predicts that a randomly generated ensemble of front waves should give rise to a linear increase of the RMS fluctuations of a crack front with time. However, Figure 8 indicates that the lack of continuous increases of either the velocity or surface height fluctuations in the present experiments. This inconsistency between the model and the experiments most likely reflects the rapid decay of front waves in the present system. Thus the “memory” of the perturbation that is excited by a given front wave decays too rapidly to generate long-lasting effects. If, on the other hand, the FWs were long-lived, the intrinsic roughness generated by them would propagate indefinitely along the front, leading eventually to the predicted increase in fracture front corrugation with time.

4. Discussion: Dynamic Fracture Effects in Granular Materials and Their Implications to Dynamic Fracture in Natural Rocks

[57] Several characteristics of dynamic fracture that have been documented in experiments on ideal (nongrainy), amorphous materials [Sharon *et al.*, 1995; Sharon and Fineberg, 1996; Livne *et al.*, 2005] have been observed in the present work. This similarity suggests that the basic dynamics of rapid fracture is universal and independent of the detailed nature of a brittle material. The grains appear to strongly affect the local (instantaneous) dynamics. These effects could be very large and have implications on the fracture of natural rocks and earthquake mechanics. Below, we will discuss these issues in detail.

4.1. Velocity Fluctuations and Irregular Fracture Fronts

[58] The local fluctuations and segmentation of the propagating fronts in our experiments are much larger than in amorphous materials [cf. Sharon *et al.*, 1995, 1996]. Rapid fractures in grainy materials exhibit large fluctuations of the instantaneous fracture velocities and segmentation of the fracture front in the Y (sample width) direction (Figure 4). These fluctuations result from (1) the interaction of fracture fronts with small-scale heterogeneities associated with the grains, (2) the formation of microbranches, and (3) by large-scale heterogeneities distributed within the sample. The dynamics of different segmented fronts can give rise to apparent anomalous velocities that exceed the Rayleigh wave speed (Figure 4). These anomalous velocities are accompanied by increasing of roughness (RMS). Segmentation of the fracture front may occur during microbranching events. Such large velocity fluctuations, first noted by Bieniawski [1967], can now be understood as the consequence of microbranching and fracture front segmentation.

[59] The abrupt velocity fluctuations, which are observed in the present experiments, suggest that, even in very simple geometries and loading configurations, the grainy characteristic of the material strongly affects the fracture velocity and the shape of the propagating fracture front. This observation could be significant in the analysis of earth-

quake dynamics. Although earthquake propagation is generally described by either frictional sliding or shear cracks [Kanamori and Brodsky, 2004], our results suggest that the heterogeneous nature of rocks could amplify both the local velocity fluctuations and the rupture front segmentation during earthquakes [Fukuyama and Madariaga, 2000]. These effects could be reflected by high frequency wave radiation emitted during earthquake propagation [Madariaga, 1983].

4.2. Branching

[60] Our experiments demonstrated that the appearance of branches and their size depends strongly on the fracture velocity. Microbranches begin to be visible when fractures propagate at average velocities where $v > 0.3 V_R$, and larger microbranches, at scales of a few mm, are observed for average velocities above $0.5V_R$. As observed in amorphous materials [Sharon *et al.*, 1996; Livne *et al.*, 2005], surface roughness and microbranches develop at relatively high velocities (Figure 6) and the velocity fluctuations increase systematically when branches appear (Figure 3a).

[61] Macrobranches, which are branches that traverse the entire sample width, did not develop in our experiments. Macrobranches did develop at average propagation velocity of about $0.5V_R$ in Norite plates in impact experiments [Bieniawski, 1967]. In the field, branched fractures have been documented when rocks from deep boreholes were unloaded [Bankwitz and Bankwitz, 1995], near large faults [Sagy *et al.*, 2001], and at extraterrestrial impact sites [Sagy *et al.*, 2002, 2004]. We thus conclude that the development of macrobranches in grainy materials requires energies, loading rates and velocities which are extremely large. A possible reason for this is that inherent graininess perturbs the long-range correlations that are a necessary condition for large-scale branching. A large degree of front segmentation, as in our experiments, would significantly deter long-range correlations and impede large-scale branching. There is an additional important effect that may inhibit the propagation of branched fractures. The numerous voids and inclusions within the rock may serve as fracture “inhibitors”, by blunting the singularity at the tip of any initially sharp fracture that encounters them. This mechanism would tend to limit the propagation of branched fractures only to the very near vicinity of the main fracture. Thus the appearance of branched fractures near large faults [e.g., Sagy *et al.*, 2001] may serve as an indication of the intense local energy release by the fault seismic activity.

4.3. Fracture Topography and Roughness

[62] Many types of fractographic features are found along tensile fractures in the field and experiments [Kulander *et al.*, 1979]. We, however, found only limited types of fractographic features in the present experiments. Characteristic mirror zones [Bahat *et al.*, 2003] were observed in our experiments (Figure 6) when the fractures were relatively slow $V < 0.3V_R$. Hackles, which are lineated twists in the fracture front, are widespread in rocks and other brittle materials when the externally applied load is induced at a point, by impact or explosion, and, therefore, are rarely observed in our experiments. In some cases we observed striations that radiate from “holes” (microbranches), which were notably different in angle and shape from the striations formed by front wave traces. These could be interpreted as

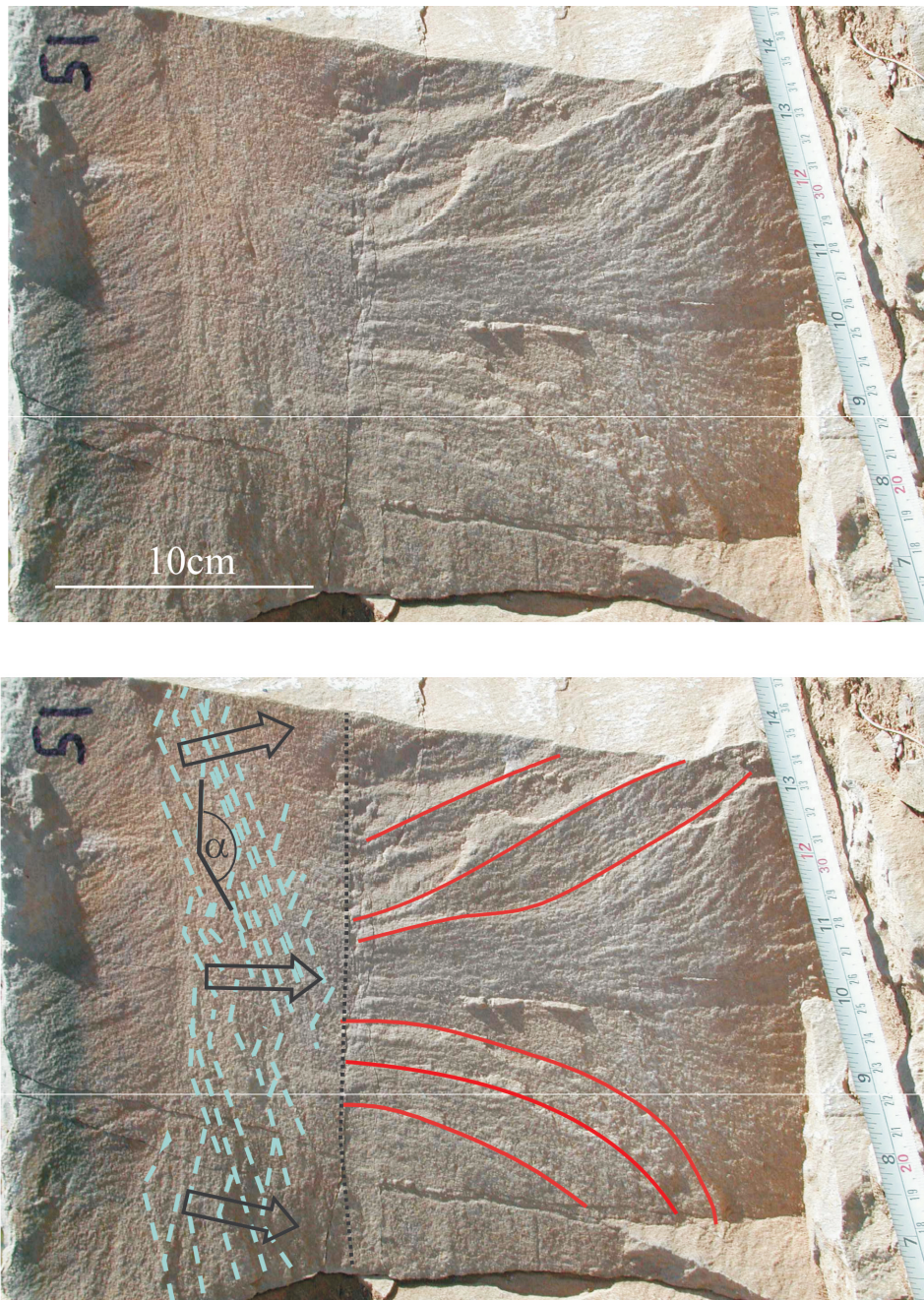


Figure 11. Surface of a joint at the Carmel formation Utah. The striations (dashed lines) are interpreted here as traces of front waves on the “mirror zone” of the joint. Using equation (5), the observed velocity is calculated as $V = 0.2V_R \approx 0.4$ km/s. The hackles (continuous lines) lines reflect twisting of the front in the Z direction, which may have been amplified when the joint crossed a preexisting joint (marked by dotted line).

hackles which developed when the fracture front symmetry was broken by a branch. Other common features, such as plumose, arrest lines, or twist hackles, do not develop in our experiments, and cannot be ascribed solely to fracture propagation velocity, at least in the presented loading/geometry configuration.

[63] Finally, our experiments suggest that surface roughness analysis can be used to identify dynamic fracture propagation. One should note, however, that the occurrence of dynamic fracture does not necessarily imply intense

roughness. For example, the mirror region of dynamic joints (before the onset of the microbranching instability) may be smoother than slower propagating joints, which may be decorated by rib marks or plumose striations.

4.4. Front Waves

[64] Front wave traces can be used to measure the fracture propagation velocity in the field as was demonstrated for shatter cones by *Sagy et al.* [2004]. As shown in the present experiments, FW traces are observed even under quasi-

static loading, and we may apply the FW method to natural joints that are formed away from impact sites and major faults. One example is the joint formation observed in the fine grain limestones of the Carmel Formation, Utah, and studied by *Reches* [1998]. The surface morphology of one of these joints is displayed in Figure 11. The left part of this surface is interpreted here as a mirror zone, and the right side is interpreted as a hackle zone. Some subtle striation pairs appear within the mirror zone of Figure 11, and in light of the present experiments, we interpret them as front wave traces. Using the geometric relationship between front waves and fracture velocity (equation (3)), the velocity of this fracture in the mirror zone is estimated as $0.2 V_R$.

[65] Single front wave traces are likely to be obscured by arrest lines, large grain sizes, hackles, plumose or branches. Therefore, in the field they can be best identified in the mirror zones of the natural joints in small-grained rock (e.g., Figure 11), but may “disappear” within the hackled regions. In these cases, statistical methods (such as the cross correlations, Figures 9 and 10) could reveal their existence.

4.5. Are Dynamic Tensile Fractures Common in Geological Environments?

[66] As discussed above, the appearance of macrobranches (large branched fractures) is not necessarily the only indication of critical dynamic fractures. Moreover, equation (6) indicates that a fracture can propagate dynamically even below the critical velocity for the microbranching instability, while its energy release rate is constant. Different types of loading, including quasi-static, can generate dynamic fractures in the field, and sometimes these dynamic fractures may decelerate. For example, consider the scenario of a force P that is applied to the edge of a crack with a blunt tip [*Freund*, 1990]. In this case, $K_I = [2P/(\pi L)]^{1/2}$, and, when the crack is overstressed, it will first accelerate as a result of the overstress, and then rapidly decelerate to zero when $L = nL_0$ (L is the length of the propagating crack, L_0 is the initial length, and n is the bluntness parameter [see *Freund*, 1990, p. 399]). We hypothesize that this analysis could explain joint and dike propagation by internal fluid pressure; related examples were discussed by *Engelder and Fischer* [1996].

[67] We conclude that dynamic fractures in rocks are more common than usually assumed, although macrobranches are less widespread [*Kulander and Dean*, 1995] and probably developed under relatively large amounts of energy. *Sagy et al.* [2001, 2004] demonstrated some unique geological environments in which branched tensile fractures are developed. We also wish to note that fractures in field may also propagate at subcritical velocities [*Segall*, 1984; *Olson*, 1993]. For example, *Müller and Dahm* [2000] showed in their experiments that plumose similar to those that observed on joints result during slow viscous propagation. Further field work and structural analysis is needed to differentiate between subcritical and dynamic fractures.

5. Summary and Conclusions

5.1. Velocity History

[68] We performed numerous experiments on dynamic fracture in rock-like granular plates that revealed the following features:

[69] 1. The propagating fractures display a similar velocity history: a stage of rapid acceleration followed by a stage of quasi-constant average velocity (Figure 3). An initial stage of relatively slow steady state propagation with $V < 0.2V_R$ observed in several experiments (Figure 3a).

[70] 2. Large fluctuations of the instantaneous velocities with associated rapid acceleration and deceleration of the propagating fracture front (Figure 3). These fluctuations appear at the stage when the average velocities increase beyond $0.3-0.5V_R$ (last stage in Figure 3), when microbranches are first observed. We interpret the fluctuations as resulting from (1) the interaction of fracture front with small-scale grain heterogeneities (small fluctuations); (2) the formation of microbranches; and (3) large-scale sample heterogeneities. The amplitudes of the velocity fluctuations increase with the increase of the average velocity (Figure 3).

[71] 3. In some cases, the velocity fluctuations are extreme; we showed that these cases indicate irregular fracture fronts that undergo either segmentation or deflection (Figure 4).

5.2. Fracture Morphology and Roughness

[72] In general microbranch size increases with the average velocity: Microbranches become visible when the host fracture propagates at average velocities of $V > 0.3 V_R$. Larger microbranches, at scales of a few millimeters developed for average velocity above $0.5 V_R$.

[73] The microbranches are arranged in bands (branch lines) which are roughly oriented along the propagation direction. These can be recognized by elongated grooves on the fracture surface (Figure 6).

[74] The development of microbranches is associated with large instantaneous velocity fluctuations; this indicates that the microbranches “break” the fracture front into segments.

[75] The amplitude of the surface topography intensifies with the increase of the average velocity. The contribution of the microbranches to the surface area is 7–12% (with respect to smooth “mirror” area). It is assumed that additional surface area is contributed by subsurface branches [*Sharon et al.*, 1996]; these subsurface branches could not be observed in the present materials.

[76] The roughness of the fracture surface, as represented by both its local amplitude and the RMS of the surface topography over the sample width, correlates well with the intensity of velocity fluctuations (Figure 8).

[77] We identify small-amplitude fracture front waves (FW) associated with the fracture propagation. The fracture velocities determined from the FW data match the average local velocity that was measured independently during the experiment.

[78] **Acknowledgments.** The authors acknowledge with many thanks the helpful conversations with T. Epstein, A. Livne, and S. M. Rubinstein. The careful reviews of J. Olson and anonymous reviewer significantly contributed to the quality of the manuscript. The study was supported by United States–Israel Binational Science Foundation, grant 98–135 and by Israel Science Fund grant 175-02. J.F. acknowledges partial support by the National Science Foundation under grant PHY99-0794.

References

- Bahat, D., P. Bankwitz, and E. Bankwitz (2003), Preuplift joints in granites: Evidence for subcritical and postcritical fracture growth, *Geol. Soc. Am. Bull.*, 115(2), 148–165.

- Bankwitz, P., and E. Bankwitz (1995), Fractographic features on joints of KBT drill cores (Bavaria Germany), in *Fractography: Fracture Topography as a Tool in Fracture Mechanics and Stress Analysis*, edited by M. S. Ameen, *Geol. Soc. Spec. Publ.*, 92, 39–58.
- Ben-Zion, Y., and J. A. Morrissey (1995), simple re-derivation of logarithmic disordering of a dynamic planar crack due to small random heterogeneities, *J. Mech. Phys. Solids*, 43, 1363–1368.
- Bieniawski, Z. T. (1967), Mechanism of brittle fracture of rock, part II experimental studies, *Int. J. Rock Mech. Min. Sci.*, 4, 407–423.
- Engelder, T., and M. P. Fischer (1996), Loading configurations and driving mechanisms for joints based on the Griffith energy-balance concept, *Tectonophysics*, 256, 253–277.
- Farmer, I. (1983), *Engineering Behaviour of Rocks*, 208 pp., CRC Press, Boca Raton, Fla.
- Fineberg, J., and M. Marder (1999), Instability in dynamic fracture, *Phys. Rep.*, 313, 2–108.
- Fineberg, J., S. P. Gross, M. Marder, and H.L. Swinney (1992), Instability in the propagation of fast cracks, *Phys. Rev. B*, 45, 5146–5154.
- Freund, L. B. (1990), *Dynamic Fracture Mechanics*, 563 pp., Cambridge Univ. Press, New York.
- Fukuyama, E., and R. Madariaga (2000), Dynamic propagation and interaction of a rupture front on a planar fault, *Pure Appl. Geophys.*, 157(11–12), 1959–1979.
- Grady, D. E., and M. E. Kipp (1987), Dynamic rock fragmentation, in *Fracture Mechanics of Rock*, edited by B. K. Atkinson, pp., 429–475, Elsevier, New York.
- Kanamori, H., and E. E. Brodsky (2004), The physics of earthquakes, *Rep. Prog. Phys.*, 67, 1429–1496.
- Kulander, B. R., and S. L. Dean (1995), Observations on fractography with laboratory experiments for geologist, in *Fractography: Fracture Topography as a Tool in Fracture Mechanics and Stress Analysis*, edited by M. S. Ameen, *Geol. Soc. Spec. Publ.*, 92, 59–82.
- Kulander, B. R., C. C. Barton, and S. L. Dean (1979), The application of fractography to core and outcrop fracture investigations, *Rep. METC/SP-79/3*, Morgantown Energy Technol. Cent., U.S. Dep. of Energy, Morgantown, W. V.
- Landau, L. D., and E. M. Lifshitz (1986), *Theory of Elasticity*, 3rd ed., 62 pp., Elsevier, New York.
- Lawn, B. (1993), *Fracture of Brittle Solids*, 2ed ed., 378 pp., Cambridge Univ. Press, New York.
- Livne, A., G. Cohen, and J. Fineberg (2005), Universality and hysteretic dynamics in rapid fracture, *Phys. Rev. Lett.*, 94, 224301.
- Madariaga, R. (1983), High-frequency radiation from dynamic earthquake fault models, *Ann. Geophys.*, 1(1), 17–23.
- Miller, O., L. B. Freund, and A. Needleman (1999), Modeling and simulation of dynamic fragmentation in brittle materials, *Int. J. Fract.*, 96, 101–125.
- Morrissey, J. W., and J. R. Rice (1998), Crack front waves, *J. Mech. Phys. Solids*, 46, 467–487.
- Morrissey, J. W., and J. R. Rice (2000), Perturbative simulations of crack front waves, *J. Mech. Phys. Solids*, 48, 1229–1251.
- Müller, G., and T. Dahm (2000), Fracture morphology of tensile cracks and rupture velocity, *J. Geophys. Res.*, 105, 723–738.
- Olson, J. E. (1993), Joint pattern development: Effects of subcritical crack growth and mechanical crack interaction, *J. Geophys. Res.*, 98, 12,251–12,265.
- Perrin, G., and J. R. Rice (1994), Disorder of a dynamic planar crack front in a model elastic medium of randomly variable toughness, *J. Mech. Phys. Solids*, 42, 1047–1064.
- Pollard, D. D., and A. Aydin (1988), Progress in understanding jointing over the past century, *Geol. Soc. Am. Bull.*, 100, 1181–1204.
- Price, N. J. (1966), *Fault and Joint Development in Brittle and Semi-Brittle Rocks*, 176 pp., Elsevier, New York.
- Ravi-Chandar, K., and W. G. Knauss (1984a), An experimental investigation into dynamic fracture. I. Crack initiation and arrest, *Int. J. Fract.*, 25, 247–267.
- Ravi-Chandar, K., and W. G. Knauss (1984b), An experimental investigation into dynamic fracture. II. Microstructural aspects, *Int. J. Fract.*, 26, 65–80.
- Ravi-Chandar, K., and W. G. Knauss (1984c), An experimental investigation into dynamic fracture. III. On steady-state crack propagation and crack branching, *Int. J. Fract.*, 26, 141–154.
- Reches, Z. (1998), Tensile fracturing of stiff rock layers under triaxial compressive stress states: 3rd NARMS, Mexico, *Int. J. Rock Mech. Min. Sci.*, 35, Paper 70.
- Sagy, A., Z. Reches, and I. Roman (2001), Dynamic fracturing; field and experimental observations, *J. Struct. Geol.*, 23, 1223–1239.
- Sagy, A., Z. Reches, and J. Fineberg (2002), Dynamic fracture by large extraterrestrial impacts as the origin of shatter-cones, *Nature*, 418, 310–313.
- Sagy, A., J. Fineberg, and Z. Reches (2004), Shatter cones: Branched, rapid fractures formed by shock impact, *J. Geophys. Res.*, 109, B10209, doi:10.1029/2004JB003016.
- Schardin, H. (1959), Velocity effects in fracture, in *Fracture*, edited by B. L. Averbach et al., pp., 297–329, John Wiley, New York.
- Segall, P. (1984), Formation and growth of extensional fracture sets, *Geol. Soc. Am. Bull.*, 95, 454–462.
- Sharon, E., and J. Fineberg (1996), Microbranching instability and the dynamic fracture of brittle materials, *Phys. Rev. B*, 54, 7128–7139.
- Sharon, E., S. P. Gross, and J. Fineberg (1995), Local crack branching as a mechanism for instability in dynamic fracture, *Phys. Rev. Lett.*, 74, 5096–5099.
- Sharon, E., S. P. Gross, and J. Fineberg (1996), Energy dissipation in dynamic fracture, *Phys. Rev. Lett.*, 76, 2117–2120.
- Sharon, E., G. Cohen, and J. Fineberg (2001), Propagating solitary waves along a rapidly moving crack front, *Nature*, 410, 68–71.
- Sharon, E., G. Cohen, and J. Fineberg (2002), Crack front waves and the dynamics of a rapidly moving crack, *Phys. Rev. Lett.*, 88, 085503.

G. Cohen and J. Fineberg, Racah Institute of Physics, Hebrew University of Jerusalem, Jerusalem, Israel.

Z. Reches, School of Geology and Geophysics, University of Oklahoma, Norman, 100 E Boyd Street, Norman, OK 73019, USA.

A. Sagy, Department of Earth and Space Sciences, University of California, Los Angeles, P.O. Box 951567, 595 Charles Young Drive East, Los Angeles, CA 90095-0000, USA. (asagy@moho.ess.ucla.edu)